# Fast and direct preparation of a genuine lattice BEC via the quantum Mpemba effect

Philipp Westhoff,[1, *] Sebastian Paeckel,[1, †] and Mattia Moroder[2, ‡]

[1]*Department of Physics, Arnold Sommerfeld Center for Theoretical Physics (ASC),*
*Munich Center for Quantum Science and Technology (MCQST),*
*Ludwig-Maximilians-Universität München, 80333 München, Germany*
[2]*School of Physics, Trinity College Dublin, College Green, Dublin 2, D02K8N4, Ireland*

We present an efficient method for dissipatively preparing a Bose-Einstein condensate (BEC) directly on a lattice, avoiding the need for a two-staged preparation procedure currently used in ultracold-atom platforms. Our protocol is based on driving the lattice-subsystem into a non-equilibrium steady state, which we show to exhibit a lattice analog of a true BEC, where the depletion can be controlled via the dissipation strength. Furthermore, exploiting a symmetry-based Mpemba effect, we analytically identify a class of simple, experimentally-realizable states that converge exponentially faster to the steady state than typical random initializations. We also show how to tune the momentum of the created high-fidelity BEC by combining superfluid immersion with lattice shaking. Our theoretical predictions are confirmed by numerical simulations of the dissipative dynamics, quantitatively assessing the speedups yielded by our protocol, as well as the fidelities of the prepared BECs.

Preparing and controlling highly-entangled states is a central goal of analog quantum simulators based on ultra-cold atoms in optical lattices. This includes, for instance, the realization of bosonic [1] and fermionic [2] Mott insulators, topological states [3–5], antiferromagnets [6], and many-body localized states [7]. Among these various experiments, a common two-stage initialization scheme is shared. The starting point is typically to prepare a BEC in a harmonic trap via several cooling stages, which is subsequently transferred into a shallow optical lattice [8]. To reduce poisoning of the BEC with unwanted excitations and quasi particles, the transfer process needs to be performed quasi-adiabatically. This constitutes a major experimental challenge, as it exposes the BEC to particle loss, decoherence, and heating originating from the ubiquitous presence of environmental channels [9]. Therefore, it is highly desirable to prepare the BEC directly on the lattice as quick as possible in order to reduce the exposition time to the environment.

In this article, we introduce a protocol to overcome this obstacle. First, we analyze a dissipative driving protocol [10, 11], and show that its steady state can be understood as the non-equilibrium lattice analog of a true BEC exhibiting correlation lengths that are significantly larger than typical, experimental lattice sizes [12]. Our proposal is based on environment-mediated hoppings, which can be implemented via superfluid immersion [13], as illustrated in Fig. 1a. Second, we apply the quantum Mpemba effect to dissipative state preparation (DSP) [14] to accelerate the relaxation towards the steady state. While the Mpemba effect originally referred to the classical non-equilibrium phenomenon of hot systems cooling down faster than warm ones [15–17], recently it has been thoroughly investigated in isolated [18–21] and open [22–27] quantum systems. Yet, open many-body systems remained elusive so far. Here, we identify a many-body quantum Mpemba effect generated by a dis-
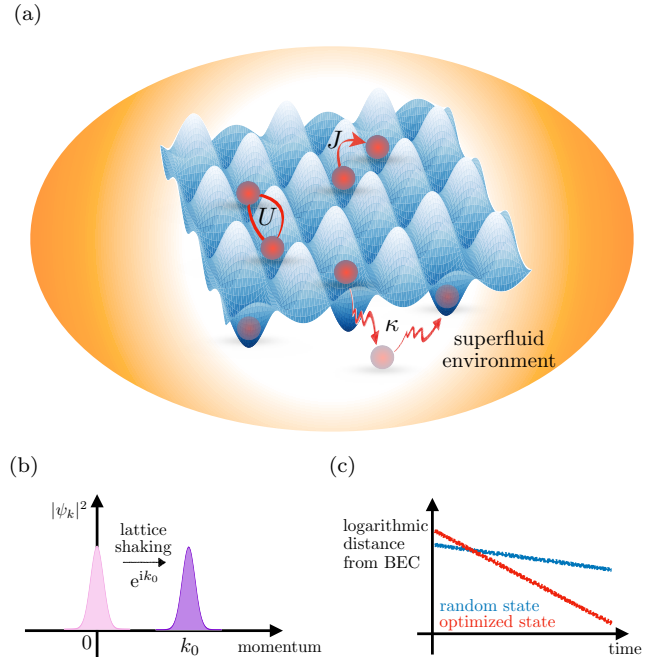


FIG. 1. Mpemba-effect-assisted preparation of a Bose-Einstein condensate (BEC) in an optical lattice. Panel a): A condensate of interacting bosonic particles can be prepared by combining coherent hopping with dissipation-mediated tunneling via a superfluid environment in which the optical lattice is immersed. Panel b): Adding a complex phase to the hoppings via lattice shaking (see main text) allows tuning the momentum of the prepared BEC. Panel c): Based on a symmetry argument, we identify a class of product states that converge exponentially faster to the target BEC.

crete symmetry of the system yielding a class of states that converge *exponentially* faster towards a BEC (i.e., the steady state), compared to previous schemes [10, 11]. We show that this speedup is realized via experimentally *easily-accessible* initial states. This approach even car-

ries over to the preparation of finite-momentum BECs, which requires the modulation of the environmentally-mediated hopping by an additional complex phase via lattice shaking techniques [28–30], depicted in Fig. 1b.

*The quantum Mpemba effect*   The dynamics of a quantum system weakly coupled to a Markovian (i.e. memoryless) environment obey the Lindblad master equation [31]

$$\frac{\mathrm{d}\hat{\rho}}{\mathrm{d}t} = \mathcal{L}\hat{\rho} = -\mathrm{i}[\hat{H}, \hat{\rho}] + \sum_l \hat{L}_l \hat{\rho} \hat{L}_l^\dagger - \frac{1}{2}\{\hat{L}_l^\dagger \hat{L}_l, \hat{\rho}\} \,, \quad (1)$$

where $[\cdot, \cdot]$ and $\{\cdot, \cdot\}$ indicate the commutator and anticommutator, respectively, $\hat{\rho}$ denotes the system's density matrix, $\hat{H}$ the Hamiltonian, and the influence of the environment is captured by so-called jump operators $\hat{L}_l$. In the eigenbasis of the Lindbladian superoperator $\mathcal{L}$, the time evolved-density matrix can be written as [23]

$$\hat{\rho}(t) = \mathrm{e}^{\mathcal{L}t}\hat{\rho}_0 = \hat{\rho}_{\mathrm{ss}} + \sum_{p=2}^{D^2} \mathrm{e}^{\lambda_p t}\mathrm{Tr}(\hat{\rho}_0 \hat{l}_p)\hat{r}_p \,. \quad (2)$$

Here, $\hat{\rho}_0$ is the initial state, $\lambda_p$ indicates an eigenvalue of $\mathcal{L}$, $\hat{l}_p$ and $\hat{r}_p$ are its corresponding left and right eigenmodes and $D$ is the dimension of $\hat{H}$. Since all $\lambda_p$ have negative real parts, every term in Eq. (2) decays exponentially in time except for the steady state $\hat{\rho}_{\mathrm{ss}}$, which, up to normalization, is given by the right eigenmode corresponding to the eigenvalue $\lambda_1$. Let us sort the eigenvalues ascendingly according to the absolute value of their real part as $\lambda_1 = 0 < |\mathrm{Re}(\lambda_2)| \le |\mathrm{Re}(\lambda_3)| \le \cdots$. At late times, a typical random state will approach the steady state with an equilibration speed $\propto \exp[\mathrm{Re}(\lambda_2)t]$. Instead, special states that have zero overlap with the so-called slowest decaying mode $\hat{l}_2$ will equilibrate exponentially faster, namely as $\exp[\mathrm{Re}(\lambda_3)t]$. Given some distance function $\mathfrak{D}$ (for instance the $L_2$-norm) and assuming that initially the special, fast-equilibrating states have a larger distance to the steady state $\hat{\rho}_{\mathrm{ss}}$ than typical, random ones, their distance curves w.r.t. $\hat{\rho}_{\mathrm{ss}}$ will cross as a function of time, which is called a Mpemba effect [16] (as illustrated in Fig. 1c).

*Preparing a lattice BEC*   We consider bosonic particles in a one dimensional (1D) lattice described by the Bose-Hubbard Hamiltonian

$$\hat{H}_{k_0} = -J\sigma_{k_0}\sum_{j=1}^{L-1}\left(\mathrm{e}^{\mathrm{i}k_0}\hat{b}_{j+1}^\dagger \hat{b}_j + \mathrm{h.c.}\right) + \frac{U}{2}\sum_{j=1}^{L}\left[\hat{b}_j^\dagger\right]^2\left[\hat{b}_j\right]^2 \,. \quad (3)$$

Here, $\hat{b}_j^\dagger$ ($\hat{b}_j$) creates (annihilates) a boson on site $j$, $L$ is the number of sites, $J$ and $U$ represent the hopping amplitude and the onsite interaction strength, and we consider open boundary conditions (OBCs). The prefactor $\sigma_{k_0}$ is 1 for $|k_0| < \pi/2$ and $-1$ otherwise, ensuring that the real part of the hopping amplitude is always negative

for $J > 0$ (we set the lattice spacing to one). We study the Markovian dissipative dynamics obeying Eq. (1) and choose

$$\hat{L}_j^{k_0} = \sqrt{\kappa}(\hat{b}_{j+1}^\dagger + \mathrm{e}^{-\mathrm{i}k_0}\hat{b}_j^\dagger)(\hat{b}_{j+1} - \mathrm{e}^{\mathrm{i}k_0}\hat{b}_j) \quad (4)$$

as jump operators with dissipation strength $\kappa$. Up to the phase factor $e^{ik_0}$, Eqs. (3) and (4) are consistent with the model proposed in [10, 11]. These jump operators drive any initial state to a BEC and can be experimentally realized by immersing the system in a superfluid [13]. Using Bogoliubov theory, we derive the steady states in each $k$-sector (see the supplementary information [32]), which are given by $\hat{\rho}_{\mathrm{ss}}^k = \mathrm{e}^{-\hat{h}_{\mathrm{eff}}/T_{\mathrm{eff}}}/Z_k$, where $\hat{h}_{\mathrm{eff}}^k = E_{\mathrm{eff}}^k \hat{a}_k^\dagger \hat{a}_k$ is an effective single-particle Hamiltonian, and $T_{\mathrm{eff}}$ can be interpreted as the effective temperature. The system's steady state can be written as $\hat{\rho}_{\mathrm{ss}} = \prod_k \hat{\rho}_{\mathrm{ss}}^k$. Expanding $E_{\mathrm{eff}}^k$ in the limit $\frac{(Un)^2}{(1+a^2)E_k^2} \gg 0$ with $E_k = \varepsilon_k\sqrt{1 + Un/(1+a^2)\varepsilon_k}$, the density $n = N/L$, and $a = 2n\kappa/J$, the effective temperature acquires a particularly simple form, which to the first non-trivial order in the dissipation strength is given by

$$T_{\mathrm{eff}} = \frac{Un}{2\sqrt{1 + (2n\kappa/J)^2}} \,. \quad (5)$$

Interestingly, in this limit, the effective $k$-Hamiltonian also simplifies and reduces to Eq. (3), when replacing the interaction $U \to \tilde{U} = U/(1+a^2)$. Note how dissipation suppresses the effective repulsive interaction, eventually generating a maximal condensation in the limit $\kappa/J \gg 1$. This starkly contrasts the equilibrium case where a true condensation is forbidden and underlines the non-equilibrium character of the steady state. In fact, our results suggest a picture in which lattice bosons scatter off the immersing BEC, yielding an effective pumping protocol. As a consequence, the effective temperatures can be significantly lower than the one of the immersing BEC, and hence, the coherence of the prepared lattice BEC much higher. To illustrate this point, we perturbatively evaluated the condensate depletion finding $\delta = (N - N_0)/N \sim \mathcal{O}((U/\kappa)^2)$, where $N_0$ denotes the occupation of the condensate, as well as the two-point correlation functions $\langle \hat{b}_i^\dagger \hat{b}_j \rangle \overset{i-j=L}{\longrightarrow} n - \mathcal{O}(U/\kappa)^2$, which we denote as a lattice analog of off-diagonal long-range order [33, 34]. Note that both quantities can be controlled by tuning $U/\kappa$. Strikingly, the condensate depletion vanishes as $(U/\kappa)^2$, which suggests that BECs with an extremely large condensate fraction can be realized. Finally, using the phase modulation $\mathrm{e}^{\mathrm{i}k_0}$, which can be implemented via lattice shaking [29, 30], i.e. by adding a fast-oscillating laser field, the mode $k_0$ in which the particles condensate can be tuned, allowing for the fast realization of high-quality finite-momentum BECs. We note that the case $k_0 = \pi$ is particularly simple to realize experimentally since $\mathrm{e}^{\mathrm{i}\pi} = -1$ implies that both the
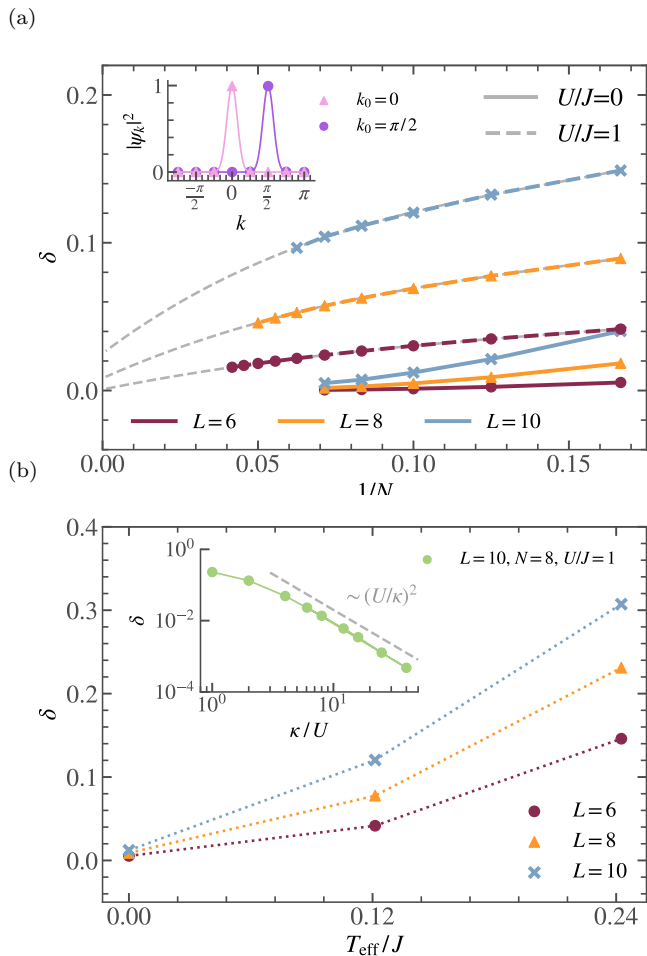
(a)



(b)

FIG. 2. Simulating the dissipative preparation of a finite-momentum BEC in a 1D lattice. Panel a): The condensate depletion as a function of the inverse total particle number $N$. The extensive scaling is clearly visible for $L = 6$ and $L = 8$, while for $N = 10$ larger particle numbers would be required. The extrapolations to $1/N \to 0$ (gray lines) were performed with a third-order polynomial in $1/N$. Inset: Momentum space representation of the eigenvector $\psi$ corresponding to the eigenvalue $N_0$ of $\boldsymbol{\gamma}$ for characteristic Lindbladian momenta $k_0 = 0$ and $k_0 = \pi/2$ (see Eq. (4)). Panel b): The condensate depletion as a function of the effective temperature defined in Eq. (5). All datasets were obtained at unit filling $N/L = 1$. Inset: $\kappa$-dependence of the depletion. We recover the $\kappa^{-2}$ scaling predicted from Bogoliubov theory. In both insets, the couplings are $U = J = 1$ with local dimension $d = N + 1$. In the upper inset, $L = 8$ and $N = 10$, while in the second one $L = 10$ and $N = 8$ were chosen. Except for the second inset, we always set $\kappa = 2J$.

coherent and the incoherent hopping are real and thus lattice shaking is not required.

*Symmetry-adapted initial states* A set of fast-converging initial states can be found without explicitly diagonalizing $\mathcal{L}$. For that purpose, we exploit the fact that the Lindbladian and its unique steady state are invariant under a (discrete) symmetry. We emphasize that here and der a (discrete) symmetry. We emphasize that here and

in the following, we refer to symmetry transformations on the vectorized, i.e., doubled, Hilbert space, which should not be confused with transformations on the physical Hilbert space only. Specifically, for $k_0 = 0$ the Lindbladian constructed from Eqs. (3) and (4) possesses the same inversion symmetry as the Hamiltonian Eq. (3), i.e. it is invariant under reflections about the center of the lattice described by the unitary transformation $\hat{U}_{\mathrm{inv}} \hat{b}_j^\dagger \hat{U}_{\mathrm{inv}}^\dagger = \hat{b}_{L+1-j}^\dagger$ [35]. This symmetry decomposes $\mathcal{L}$ into two blocks, corresponding to eigenmodes that transform evenly or oddly under $\tilde{U}_{\mathrm{inv}}$. We investigate the unitary part of the Lindbladian $\mathcal{H}$ (see Eq. (1)), which in its vectorized form is given by $\hat{\mathcal{H}} = -\mathrm{i}\hat{H} \otimes \hat{\mathbb{1}} + \hat{\mathbb{1}} \otimes \mathrm{i}\hat{H}^T$ [36]. In the supplementary information, [32] we show that its vectorized eigenstates are adiabatically connected to those of $\mathcal{L}$ using perturbation theory in the limit $\kappa \to 0^+$. We furthermore find that the slowest-decaying mode $\hat{l}_2$ always transforms oddly under inversion. An important consequence of the previous considerations is that any physically-realizable state that is symmetric under reflections about the center of the lattice has zero overlap with $\hat{l}_2$ and equilibrates exponentially faster to the BEC than random initial states. This also includes the product states

$$|\psi\rangle = |n_1, n_2, \ldots, n_{L/2}, n_{L/2}, \ldots n_2, n_1\rangle \,, \qquad (6)$$

where $n_j$ indicates the number of particles on site $j$. Common examples of states of the type Eq. (6) include so-called wedding-cake states $|\psi\rangle = |1, 2, \ldots, L/2 - 1, L/2, L/2, L/2 - 1, \ldots, 2, 1\rangle$, which can be readily prepared in harmonic traps. Among such symmetric, fast-converging product states, the fastest-converging is the one where all particles are initially located on the central site(s) [37]. This can be qualitatively understood from the fact that such a state is connected to the BEC by a minimal number of hoppings and we call it the symmetrically-localized (SL) state. Crucially, the SL state can also be realized experimentally in the novel hybrid setups combining optical lattices with optical tweezers [38, 39]. However, we want to point out that all states of the form Eq. (6) exhibit exponential speedups. Note that the same symmetry arguments can be applied to higher-dimensional systems, and preliminary numerical evidence shows that the SL state is the fastest-converging one also in 2D.

The arguments outlined above directly apply to the zero momentum case $k_0 = 0$, only. However, Lindbladians with different characteristic momenta $k_0$ (see Eq. (4)) and their eigenmodes are unitarily connected to one another, as we discuss in the supplementary information [32].

*Simulating the dissipative dynamics* To explicitly study the validity range of the large $\kappa/J$-expansion of the steady state $\hat{\rho}_{\mathrm{ss}}$, and to test the exponentially faster convergence of the proposed initial states Eq. (6), we
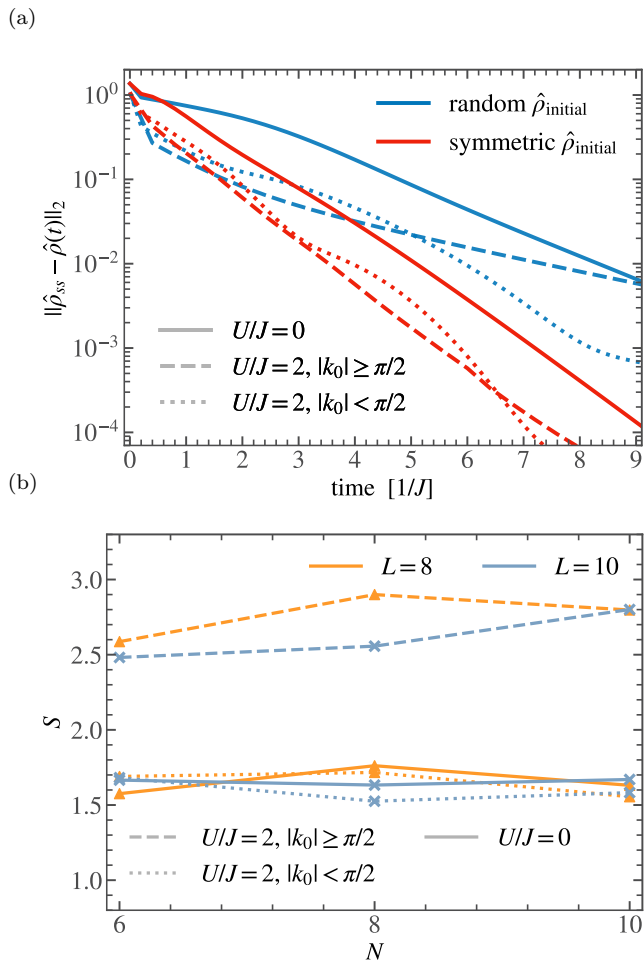
(a)



(b)



FIG. 3. Mpemba-speedups in the preparation of BECs. Panel a): The symmetrically-localized (SL) state (red lines), where all particles are initially located on the central site(s), converges exponentially faster to the steady state $\hat{\rho}_{ss}$ than random initial product states (blue lines). Random states are generated by distributing $N$ particles on the lattice, sampling the positions from a uniform distribution over the sites. Line styles indicate different bosonic interaction strengths and characteristic momenta $k_0$. All calculations were performed with system parameters $L = 10$, $N = 10$, local dimension $d = N + 1$, and $\kappa = 2J$, and we averaged over 5 product state realizations. Panel b): The corresponding speedups $S = t_{\text{random}}/t_{\text{symmetric}}$ as a function of the total particle number. $t_{\text{random}}$ and $t_{\text{symmetric}}$ are the times at which the $L_2$-distance from the steady state has dropped below a precision threshold $\epsilon = 10^{-4}$ for the random and the SL states, respectively.

employ matrix-product state (MPS) techniques to numerically compute the dissipative evolution induced by Eq. (1) for 1D many-body systems. We represent vectorized density matrices as matrix-product states (MPSs) [40] and vectorized Lindbladians as matrix-product operators (MPOs) [41]. The time evolution is computed with a variant of the time-dependent variational prin-

ciple (TDVP) [42, 43] tailored for bosonic systems (see the supplementary information [32] for the details of the numerical implementation).

First, in Fig. 2 we show the accuracy of the obtained BECs at different momenta. For this purpose, we compute the condensate depletion $\delta$ as the deviation of the leading eigenvalue $N_0$ of the one-body density matrix $\boldsymbol{\gamma}$, componentwise defined via $\boldsymbol{\gamma}_{ij} = \langle \hat{b}_j^\dagger \hat{b}_i \rangle$, from the maximal possible condensate population $N$. Fig. 2a shows that the condensate depletion decreases upon increasing the total particle number $N$ and we find an extensive scaling $\delta \sim \mathcal{O}(1/N)$, in agreement with the Bogoliubov theory. Noteworthy, extrapolating the condensate depletion as a function of $1/N$ to the limit $N \to \infty$, we observe $\delta \to 0$ also at finite interaction strengths $U/J = 1$ (dashed lines). Moreover, the inset indicates that the eigenvector corresponding to the leading eigenvalue of $\boldsymbol{\gamma}$ has almost unit weight at the characteristic momentum of the Lindbladian $k_0$, demonstrating the formation of a finite-momentum BEC, controlled by $k_0$. Next, in Fig. 2b, we show that the condensate depletion increases with the effective temperature $T_{\text{eff}}$. In fact, if we take a typical value $J = 1$kHz for ultracold atoms, Fig. 2b indicates the formation of a condensate with depletion $\delta \sim 0.1$ for temperatures of about 10nK. Note that the inset confirms the validity of our perturbative arguments: Even for moderate values of the dissipation strength, we observe the expected scaling of the depletion $\sim (U/\kappa)^2$.

Next, we investigate the Mpemba speedups yielded by our protocol, simulating a lattice loaded with either the SL state or random product states and different values of $U/J$. In Fig. 3a, we compare the equilibration dynamics towards the BEC. As a distance measure, we consider the $L_2$-norm $\mathfrak{D}(t) = \|\hat{\rho}(t) - \hat{\rho}_{\text{ss}}\|_2$, which is the easiest to compute in the vectorized framework. We find that the SL state converges exponentially faster than random product states for all considered bosonic repulsion strengths $U/J$. Taking a more practical perspective, the actual speedup to achieve a certain condensate fidelity is the relevant quantity. For that purpose, Fig. 3b shows the corresponding speedups $S$ relative to a desired $L_2$-distance $\epsilon$ from the steady state $\hat{\rho}_{\text{ss}}$. Notably, the speedups do not change significantly when varying the system size or the number of particles. This indicates that similar speedups can also be achieved for larger system sizes. Note that due to unitary equivalence, the speedups are the same for all $|k_0| < \pi/2$ and for all $|k_0| \geq \pi/2$ [32].

*Summary/Outlook* The initialization process of loading ultracold atoms into optical lattices is a delicate procedure and its quality mostly determines the possible subsequent operations. In this work, we studied a model for dissipatively preparing a finite-momentum BEC with wave vector $k_0$, directly on the lattice. In the limit of strong dissipation, we derived an expansion of the steady state, as well as the corresponding Bogoliubov Hamiltonian. Therefrom, we obtained the asymptotic behavior of

the condensate depletion $\delta$ as well as the effective temperature, which we checked against numerical simulations. Our findings indicate that genuine lattice BECs, which, on the length scales of the lattice, are indistinguishable from true long-ranged ordered states, can be prepared very efficiently with a quadratic scaling of the depletion in the dissipation strength $\delta \sim \mathcal{O}((U/\kappa)^2)$. In order to reduce the relaxation time scales towards the steady state, we proposed an optimized protocol for preparing such lattice-BECs. For that purpose, we exploit the quantum-Mpemba effect to find fast-converging initial states exhibiting a particularly simple structure when it comes to practical realizations. We find that the case of repulsive onsite interaction $U > 0$ with $|k_0| \geq \pi/2$ provides the largest speedups, i.e., $\sim 3\times$ faster than random states, to reach a fidelity of $10^{-4}$ with respect to the steady state,

We believe that our protocol will help to significantly increase the efficiency of preparing lattice BECs, which constitutes the standard initialization procedure for all subsequent adiabatic protocols to generate highly entangled quantum states in optical lattices. Especially the fact that a so far two-staged loading procedure for the lattice BEC can be reduced to a single experimental operation, and sped up exponentially by a proper choice of experimentally easy-to-prepare initial states, promises a drastic reduction of coherence losses. From a theoretical point of view, our symmetry-based approach to find fast-converging initial states is very general and can be applied to a wide class of open quantum systems. This circumvents the necessity to diagonalize the generator and thus paves the way to finding further useful applications of the quantum Mpemba effect.

* p.westhoff@physik.uni-muenchen.de
† sebastian.paeckel@physik.uni-muenchen.de
‡ moroderm@tcd.ie

[1] M. Greiner, O. Mandel, T. Esslinger, T. W. Hänsch, and I. Bloch, Nature **415**, 39 (2002).
[2] R. Jördens, N. Strohmaier, K. Günter, H. Moritz, and T. Esslinger, Nature **455**, 204 (2008).
[3] M. Aidelsburger, M. Atala, M. Lohse, J. T. Barreiro, B. Paredes, and I. Bloch, Phys. Rev. Lett. **111**, 185301 (2013).
[4] G. Jotzu, M. Messer, R. Desbuquois, M. Lebrat, T. Uehlinger, D. Greif, and T. Esslinger, Nature **515**, 237 (2014).
[5] C. Schweizer, F. Grusdt, M. Berngruber, L. Barbiero, E. Demler, N. Goldman, I. Bloch, and M. Aidelsburger, Nature Physics **15**, 1168 (2019).
[6] R. A. Hart, P. M. Duarte, T.-L. Yang, X. Liu, T. Paiva, E. Khatami, R. T. Scalettar, N. Trivedi, D. A. Huse, and R. G. Hulet, Nature **519**, 211 (2015).
[7] M. Schreiber, S. S. Hodgman, P. Bordia, H. P. Lüschen, M. H. Fischer, R. Vosk, E. Altman, U. Schneider, and I. Bloch, Science **349**, 842 (2015).
[8] K. B. Davis, M. O. Mewes, M. R. Andrews, N. J. van Druten, D. S. Durfee, D. M. Kurn, and W. Ketterle, Phys. Rev. Lett. **75**, 3969 (1995).
[9] M. Schlosshauer, Physics Reports **831**, 1–57 (2019).
[10] S. Diehl, A. Micheli, A. Kantian, B. Kraus, H. P. Büchler, and P. Zoller, Nature Physics **4**, 878 (2008).
[11] B. Kraus, H. P. Büchler, S. Diehl, A. Kantian, A. Micheli, and P. Zoller, Phys. Rev. A **78**, 042307 (2008).
[12] F. Gyger, M. Ammenwerth, R. Tao, H. Timme, S. Snigirev, I. Bloch, and J. Zeiher, Phys. Rev. Res. **6**, 033104 (2024).
[13] A. Griessner, A. J. Daley, S. R. Clark, D. Jaksch, and P. Zoller, Phys. Rev. Lett. **97**, 220403 (2006).
[14] F. Verstraete, M. M. Wolf, and J. Ignacio Cirac, Nature Physics **5**, 633 (2009).
[15] E. B. Mpemba and D. G. Osborne, Phys. Educ. **4**, 172 (1969).
[16] Z. Lu and O. Raz, Proceedings of the National Academy of Sciences **114**, 5083 (2017).
[17] A. Kumar and J. Bechhoefer, Nature **584**, 64 (2020).
[18] F. Ares, S. Murciano, and P. Calabrese, Nat. Commun. **14**, 2036 (2023).
[19] S. Liu, H.-K. Zhang, S. Yin, and S.-X. Zhang, Phys. Rev. Lett. **133**, 140405 (2024).
[20] L. K. Joshi, J. Franke, A. Rath, F. Ares, S. Murciano, F. Kranzl, R. Blatt, P. Zoller, B. Vermersch, P. Calabrese, C. F. Roos, and M. K. Joshi, Phys. Rev. Lett. **133**, 010402 (2024).
[21] C. Rylands, K. Klobas, F. Ares, P. Calabrese, S. Murciano, and B. Bertini, Phys. Rev. Lett. **133**, 010401 (2024).
[22] A. Nava and M. Fabrizio, Phys. Rev. B **100**, 125102 (2019).
[23] F. Carollo, A. Lasanta, and I. Lesanovsky, Phys. Rev. Lett. **127**, 060401 (2021).
[24] A. K. Chatterjee, S. Takada, and H. Hayakawa, Phys. Rev. Lett. **131**, 080402 (2023).
[25] M. Moroder, O. Culhane, K. Zawadzki, and J. Goold, Phys. Rev. Lett. **133**, 140404 (2024).
[26] J. Zhang, G. Xia, C.-W. Wu, T. Chen, Q. Zhang, Y. Xie, W.-B. Su, W. Wu, C.-W. Qiu, P.-X. Chen, W. Li, H. Jing, and Y.-L. Zhou, Nature Communications **16**, 301 (2025).
[27] I. Medina, O. Culhane, F. C. Binder, G. T. Landi, and J. Goold, (2024), arXiv:2412.13259 [quant-ph].
[28] M. Di Liberto, O. Tieleman, V. Branchina, and C. M. Smith, Phys. Rev. A **84**, 013607 (2011).
[29] C. E. Creffield, G. Pieplow, F. Sols, and N. Goldman, New Journal of Physics **18**, 093013 (2016).
[30] A. Impertro, S. Huh, S. Karch, J. F. Wienand, I. Bloch, and M. Aidelsburger, (2024), arXiv:2412.09481 [cond-mat.quant-gas].
[31] G. Lindblad, Communications in Mathematical Physics **48**, 119 (1976).

[32] See Supplemental Material at [URL will be inserted by publisher], for details on the fast-converging symmetric states and on the numerical implementation of the dissipative dynamics.

[33] O. Penrose and L. Onsager, Phys. Rev. **104**, 576 (1956).

[34] C. N. Yang, Rev. Mod. Phys. **34**, 694 (1962).

[35] The more general case is covered in section S2 in [32].

[36] G. T. Landi, D. Poletti, and G. Schaller, Rev. Mod. Phys. **94**, 045006 (2022).

[37] This refers to the case of an odd number of sites $L$. In the case of an even $L$, the fastest-converging state is the one where all particles are distributed evenly between the two central sites.

[38] A. W. Young, W. J. Eckner, N. Schine, A. M. Childs, and A. M. Kaufman, Science **377**, 885 (2022), https://www.science.org/doi/pdf/10.1126/science.abo0608.

[39] R. Tao, M. Ammenwerth, F. Gyger, I. Bloch, and J. Zeiher, Phys. Rev. Lett. **133**, 013401 (2024).

[40] S. Wolff, A. Sheikhan, and C. Kollath, SciPost Phys. Core **3**, 010 (2020).

[41] H. P. Casagrande, D. Poletti, and G. T. Landi, Computer Physics Communications **267**, 108060 (2021).

[42] J. Haegeman, J. I. Cirac, T. J. Osborne, I. Pižorn, H. Verschelde, and F. Verstraete, Phys. Rev. Lett. **107**, 070601 (2011).

[43] M. Yang and S. R. White, Phys. Rev. B **102** (2020).

Philipp Westhoff,[1, *] Sebastian Paeckel,[1, †] and Mattia Moroder[2, ‡]

[1]*Department of Physics, Arnold Sommerfeld Center for Theoretical Physics (ASC),*
*Munich Center for Quantum Science and Technology (MCQST),*
*Ludwig-Maximilians-Universität München, 80333 München, Germany*
[2]*School of Physics, Trinity College Dublin, College Green, Dublin 2, D02K8N4, Ireland*

## S1. EXPONENTIALLY FASTER CONVERGING PRODUCT STATES

In this section, we prove that the symmetric states considered in the main text converge exponentially faster to the steady state than random states. Here, we first consider the special case of the zero-momentum condensate. Then, in Section S2 we generalize this result to finite momenta.

Consider the Bose Hubbard Hamiltonian at $k_0 = 0$

$$\hat{H} = -J \sum_{j=1}^{L-1} \left( \hat{b}_{j+1}^\dagger \hat{b}_j + \text{h.c.} \right) + \frac{U}{2} \sum_{j=1}^{L} \hat{b}_j^{\dagger 2} \hat{b}_j^2 , \quad (S1)$$

that we analyzed in the main text. It features a discrete symmetry that we label *inversion symmetry*, represented by the unitary $\hat{U}_{\text{inv}}$ with action

$$\hat{U}_{\text{inv}} \hat{b}_j^\dagger \hat{U}_{\text{inv}}^\dagger = \hat{b}_{L+1-j}^\dagger . \quad (S2)$$

In the case of vanishing interaction $U = 0$, the transformation

$$\hat{d}_k^\dagger = \sum_{j=1}^{L} \sin kj \, \hat{b}_j^\dagger , \quad k(m) = \frac{\pi}{L+1} m, \ m \in \{1, \ldots, L\} \quad (S3)$$

brings the Hamiltonian into the diagonal form

$$\hat{H} = -J \sum_k E_k \hat{d}_k^\dagger \hat{d}_k, \qquad E_k = 2\cos(k) . \quad (S4)$$

The eigenvectors are constructed by successively adding particles $\hat{d}_k^\dagger$ into the system. They are characterized by a vector $\mathbf{n} = (n_1, n_2, \ldots, n_L)$, which describes the occupation of each of the modes $m$,

$$|\mathbf{n}\rangle = \prod_{m=1}^{L} \frac{(\hat{d}_{k(m)}^\dagger)^{n_m}}{\sqrt{n_m!}} |0\rangle . \quad (S5)$$

---

* p.westhoff@physik.uni-muenchen.de
† sebastian.paeckel@physik.uni-muenchen.de
‡ moroderm@tcd.ie

The corresponding eigenvalues read

$$E(\mathbf{n}) = \sum_{m=1}^{L} E_{k(m)} n_m , \quad (S6)$$

and obey

$$E_{k(m)} = -E_{k(L+1-m)} . \quad (S7)$$

Moreover, the eigenvectors are also eigenvectors of the inversion symmetry $\hat{U}_{\text{inv}}$, and their eigenvalue is alternating, i.e

$$\hat{U}_{\text{inv}} \hat{d}_{k(m)}^\dagger \hat{U}_{\text{inv}}^\dagger = (-1)^{m-1} \hat{d}_{k(m)}^\dagger . \quad (S8)$$

Note that Eq. (S7) stems from the cosine in the eigenvalues and Eq. (S8) from properties of the sine. This implies that

$$\hat{U}_{\text{inv}} |\mathbf{n}\rangle = |\mathbf{n}\rangle \prod_{m=1}^{L} (-1)^{n_m(m-1)} , \quad (S9)$$

which reduces calculating the transformation behavior of a many-body state to counting the number of particles in each mode and then multiplying all their eigenvalues.

In order to study the Lindbladian, it is necessary to consider the enlarged, vectorized Hilbert space. The general form of the vectorized Lindbladian [1] is given by

$$\hat{\mathcal{L}} = \underbrace{-\mathrm{i}\hat{H} \otimes \hat{\mathbb{1}} + \hat{\mathbb{1}} \otimes \mathrm{i}\hat{H}^T}_{\hat{\mathcal{H}}} +$$
$$\underbrace{\sum_l \hat{L}_l \otimes \left(\hat{L}_l^\dagger\right)^T - \frac{1}{2}\hat{L}_l^\dagger \hat{L}_l \otimes \hat{\mathbb{1}} - \frac{1}{2}\hat{\mathbb{1}} \otimes \left(\hat{L}_l^\dagger \hat{L}_l\right)^T}_{\hat{\mathcal{D}}} . \quad (S10)$$

For $k_0 = 0$, the jump operators are

$$\hat{L}_j = \sqrt{\kappa}(\hat{b}_{j+1}^\dagger + \hat{b}_j^\dagger)(\hat{b}_{j+1} - \hat{b}_j) , \quad (S11)$$

where $\kappa$ is the dissipation strength. In the following, we focus on the unitary part of the Lindbladian $\hat{\mathcal{H}}$ which satisfies

$$\hat{\mathcal{H}} |\mathbf{n}\rangle \otimes |\tilde{\mathbf{n}}\rangle = -\mathrm{i}\big(E(\mathbf{n}) - E(\tilde{\mathbf{n}})\big) |\mathbf{n}\rangle \otimes |\tilde{\mathbf{n}}\rangle . \quad (S12)$$

For clarity, we will label the quantum number on the physical lattice $k_p$ and on the auxiliary $k_a$. Notice,
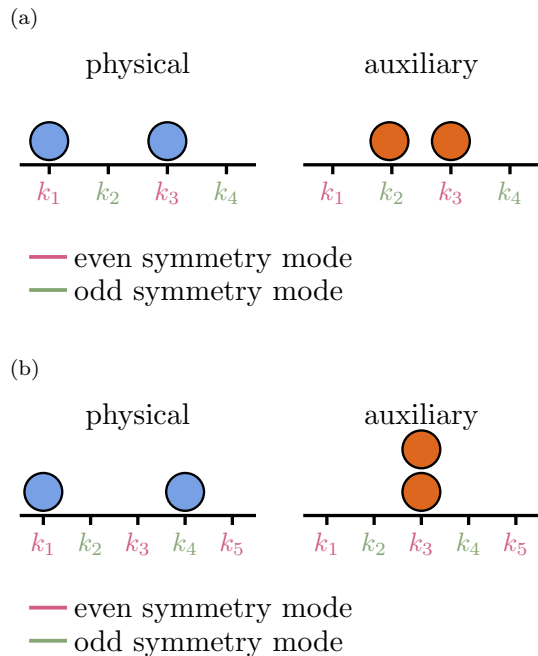
(a)



(b)



FIG. S1. Two states in the eigen-subspace of $\hat{\mathcal{H}}$ to eigenvalue $-\mathrm{i}(E_{k(1)} - E_{k(2)})$ for an even (panel a) and odd (panel b) number of sites $L$. Notice, that both states transform evenly, easily seen by the transformation behavior of every individual particle and Eq. (S9). Interestingly, in the odd-$L$ case, the $k_{L+1/2}$ mode has energy zero, which leads to a case distinction between even and odd $L$ in the proofs presented in this section.

however, that the physical states in this enlarged Hilbert space have to satisfy the constraint of equal total particle number on both the physical and auxiliary lattices. Thus, eigenvectors obey $\|\mathbf{n}\|_1 = \|\tilde{\mathbf{n}}\|_1$. The generalization of the inversion symmetry to the vectorized space reads $\hat{\mathcal{U}}_{\mathrm{inv}} = \hat{U}_{\mathrm{inv}} \otimes \hat{U}_{\mathrm{inv}}^*$. We depict examples of even and odd vectorized states in Fig. S1. With these preliminary considerations at hand, we can prove the following important observation about a certain eigenspace of $\hat{\mathcal{H}}$.

*1. Theorem*: Let $|\psi\rangle\!\rangle$ be an eigenstate of $\hat{\mathcal{H}}$ to eigenvalue $-\mathrm{i}(E_{k(1)} - E_{k(2)})$. Then it transforms oddly under inversion, that is $\hat{\mathcal{U}}_{\mathrm{inv}}|\psi\rangle\!\rangle = -|\psi\rangle\!\rangle$.

If this theorem is proven, we know that symmetric states do not have any overlap with this subspace.

*Proof of 1*: We may take a general ket in the subspace with eigenvalue $-\mathrm{i}(E_{k(1)} - E_{k(2)})$, characterized by $\mathbf{n}$ and $\tilde{\mathbf{n}}$. This eigenvalue can only be obtained if all but two particles contribute a sum of 0 to the eigenvalue, while the remaining two have exactly the eigenvalue of interest (see Eq. (S12)). Thus, we can reduce to the case with two physical and two auxiliary particles, but additionally we need to prove, that states with

eigenvalue 0 transform evenly (proven in theorem 2). Lets first focus on the former.

For two particles (that means two physical and two auxiliary ones), two particles need to create the energy difference. Consequently, the possible fillings are: $k_p(1)$ and $k_p(L - 1)$; $k_a(L)$ and $k_a(2)$; $k_p(1)$ and $k_a(2)$; $k_p(L-1)$ and $k_a(L)$ (the last two stem from the special symmetry of the dispersion relation). In the case of even $L$, the first two transform evenly, the last two oddly. For odd $L$, all transform oddly. The two remaining particles combined need to have energy 0. If this is achieved by one particle on the physical and one on the auxiliary lattice, the two particles need to occupy $k_a(m)$ and $k_p(m)$, and thus transform evenly. If they both sit in one lattice, they need to occupy $k_{r/a}(m)$ and $k_{r/a}(L+1-m)$ and together transform oddly in the case of even $L$, and evenly for odd $L$. In total, all possibilities transform oddly according to Eq. (S9).

To conclude the proof, we need the following theorem.

*2. Theorem*: Let $|\psi\rangle\!\rangle$ be an eigenstate of $\hat{\mathcal{H}}$ to eigenvalue 0. Then it transforms evenly under inversion, that is, $\hat{\mathcal{U}}_{\mathrm{inv}}|\psi\rangle\!\rangle = |\psi\rangle\!\rangle$.

*Proof of 2*: We will first reduce the general particle number case to the case with one or two particles. The eigenvalue can be rewritten as

$$E(\mathbf{n}) - E(\tilde{\mathbf{n}}) = \sum_{m=1}^{\lfloor \frac{L}{2} \rfloor} \left( n_m - \tilde{n}_m - n_{L+1-m} + \tilde{n}_{L+1-m} \right) E_{k(m)} .$$
(S13)

The left side vanishes under the condition

$$n_m - \tilde{n}_m - n_{L+1-m} + \tilde{n}_{L+1-m} = 0, \quad \forall m \leq \left\lfloor \frac{L}{2} \right\rfloor . \quad \text{(S14)}$$

Only in the case of odd $L$ there is the subtlety that $n_{L+1/2} - \tilde{n}_{L+1/2}$ might be nonzero, as $E_{L+1/2} = 0$ already. From now on, the $k$-sites $m$ and $L + 1 - m$ on the physical and auxiliary lattice together will be called $m$-th *sector*. In each of the sectors, the constraints must be fulfilled (with the exception of the $L+1/2$, which we will refer to as *zero-sector*).

This also entails an *even* number of particles in each sector. Since the energies are incommensurable, there always exist two particles that contribute a combined eigenvalue of 0. So, either one is on the physical lattice and one on the auxiliary lattice, or both are on the same lattice. In the latter case, we also need two particles on the other lattice that have eigenvalue zero. Taking away these 2 or 4 particles, we end up with a physical state with $N - 1$ or $N - 2$ particles that have the same eigenvalue. The 2 or 4 particles taken out also had eigenvalue 0, so by lemma 3 below, it transforms evenly. Doing this successively until no particles are left, the problem is reduced to the two and one-particle case,

which is the content of the next Lemma.

*3. Lemma*: Theorem 2 holds in the case of one and two (physical) particles.

*Proof of 3*: We will make a case distinction between even and odd numbers of sites $L$. Starting with an *even* number of sites and one (physical) particle, to fulfill the subspace constraint, the physical and the auxiliary particle need to sit in the same sector, denoted by $m$. It reads

$$n_m + \tilde{n}_{L+1-m} = n_{L+1-m} + \tilde{n}_m = 1 \,, \qquad \text{(S15)}$$

giving the possibilities $n_m = \tilde{n}_m = 1$ or $n_{L+1-m} = \tilde{n}_{L+1-m} = 1$, and both possible configurations transform evenly.

For two physical particles, there are more possible fillings. Either all 4 particles (2 physical and 2 auxiliary) are loaded in one sector, or two sectors are filled with two particles each. In the former case, the subspace constraint enforces

$$n_m + \tilde{n}_{L+1-m} = n_{L+1-m} + \tilde{n}_m = 2 \qquad \text{(S16)}$$

for one sector $m$, which gives rise to the fillings $n_m = \tilde{n}_m = 2$, $n_{L+1-m} + \tilde{n}_{L+1-m} = 2$, $n_m = \tilde{n}_m = n_{L+1-m} = \tilde{n}_{L+1-m} = 1$, all transforming evenly. Next, there is also the possibility of just two particles sitting in the same subspace. Now, there are two subcases: First, in each of the filled sectors, one physical and one auxiliary particle is placed, or two physical particles are placed in one sector and two auxiliary particles in the other. The first case is just two times the one particle case discussed above, and thus, it gives rise to even states. The second case however is different; if the two occupied sectors are labeled by $m$ and $r$, the constraint translates to

$$n_m = n_{L+1-m} = 1, \qquad \tilde{n}_r = \tilde{n}_{L+1-r} = 1 \,, \qquad \text{(S17)}$$

which also transforms evenly. This concludes the discussion in the case of an even number of sites.

For odd $L$, the case distinction above stays valid (although the arguments, why in each case the state transforms evenly, change). However, due to the subtlety of the zero-sector and $E_{k(L+1/2)} = 0$, particles can sit in the mode $k(L+1/2)$ without fulfilling any constraint. Luckily, to satisfy the other sector constraints, an even number of particles has to sit in this zero-sector (as the physical plus auxiliary particle number is even). Consequently, either all particles are in the zero-sector, or two particles are in there, and the remaining two particles need to obey the fillings discussed in the one-particle case. So, as every single particle in the zero-sector has odd symmetry (but an even number of them is in there), we only get even symmetry states.

Now, before this theorem is used, a neat symmetry property of the Lindbladian needs to be shown.

*4. Theorem*: The Lindbladian preserves the inversion symmetry $\hat{\mathcal{U}}_{\text{inv}}$.

This is immediately clear for the Hamiltonian part. For the dissipator, however, we have

$$\hat{U}_{\text{inv}} \hat{L}_j \hat{U}_{\text{inv}}^\dagger = \hat{U}_{\text{inv}} \sqrt{\kappa} (\hat{b}_{j+1}^\dagger + \hat{b}_j^\dagger) \hat{U}_{\text{inv}}^\dagger \hat{U}_{\text{inv}} (\hat{b}_{j+1} - \hat{b}_j) \hat{U}_{\text{inv}}^\dagger$$
$$= \sqrt{\kappa} (\hat{b}_{L-j}^\dagger + \hat{b}_{L-j+1}^\dagger)(\hat{b}_{L-j} - \hat{b}_{L-j+1}) = -\hat{L}_{L-j} \,, \qquad \text{(S18)}$$

which shows preservation of symmetry, as in the dissipator only products of two jump operators exist, and a sum over all sites is performed.

Now we can bring everything together to conclude our final theorem.

*5. Main theorem*: Consider the Lindbladian with $k_0 = 0$. All left eigenmodes, which, when adiabatically switching on the dissipation, stem from the eigenspace of $\hat{\mathcal{H}}$ to eigenvalue $-\mathrm{i}(E_{k(1)} - E_{k(2)})$, will have zero overlap with symmetric states.

*Proof of 5*: Let $\hat{l}_m$ be an eigenmode coming out of the eigenspace $-\mathrm{i}(E_{k(1)} - E_{k(2)})$. That is, there is a $\hat{l}_m^{\text{appr.}}$ in this subspace which agrees with $\hat{l}_m$ in the case of vanishing dissipation $\kappa \to 0^+$.. Such an approximate mode is found by (degenerate) perturbation theory and we can therefore safely say that $\mathrm{Tr}\big(\hat{l}_m^\dagger \hat{l}_m^{\text{appr.}}\big) \neq 0$ also for strong dissipation (see Fig. S2). But since the approximate mode lives in a space spanned by solely antisymmetric states due to theorem 1, $\hat{l}_m$ has an antisymmetric component. However, the Lindbladian preserves the inversion symmetry, so that the left eigenmodes can be chosen as eigenvectors of $\hat{\mathcal{U}}_{\text{inv}}$. We conclude that $\hat{l}_k$ has to be antisymmetric and thus has vanishing overlap with symmetric states.

Notice, that since oddly transforming states are traceless, all physical states have a evenly transforming component. Luckily, there are density matrices that transform evenly, making them orthogonal to eigenmodes coming out of the eigenspace discussed above.

Unfortunately, the main theorem tells nothing about the location of the eigenvalues corresponding to these left eigenmodes. However, we performed extensive numerical analysis for a wide range of parameters, which showed that the slowest-decaying mode always stems from this subspace. One representative example of this analysis is shown in Fig. S2, for the imaginary part of the eigenvalues (panel a) and the left eigenmodes (panel b). This explains the exponential speedup of symmetric states. It has to be said, that all the arguments also apply to the subspace $\mathrm{i}(E_{k(2)} - E_{k(1)})$, where $\hat{l}_2^\dagger$ stems from. Furthermore, there are other eigensubspaces, which only feature oddly transforming states.

This concludes the analysis in the case of $U = 0$. In the case of finite, but small on-site interaction, we can
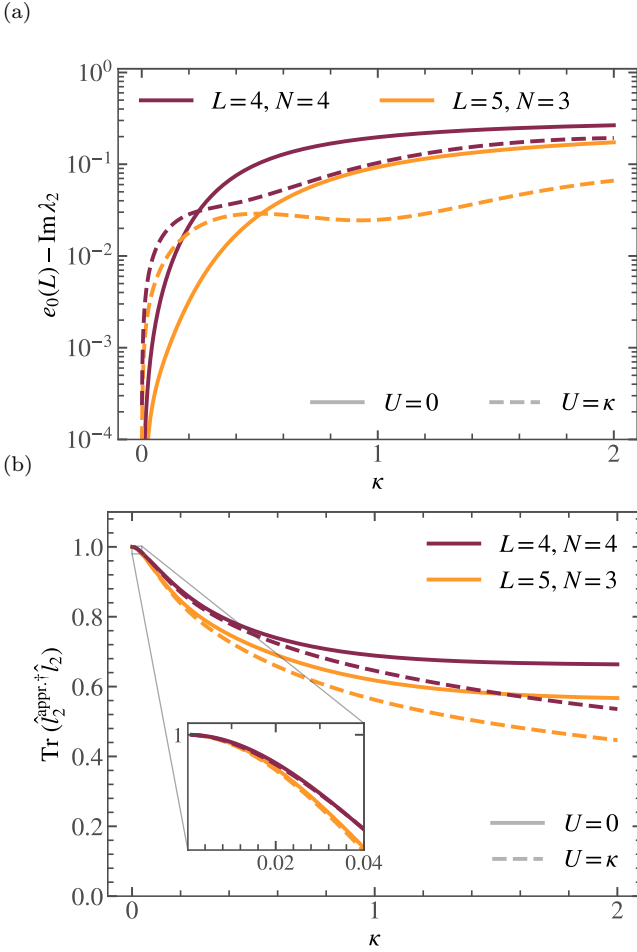
FIG. S2. Characteristics of the slowest decaying mode for different system parameters. Panel a): Difference of $\mathrm{Im}\lambda_2$ to the subspace eigenvalue $e_0(L) = E_{k(2)} - E_{k(1)}$ (see Eqs. (S4) and (S12)), which vanishes as $\kappa \to 0^+$. Panel b): Overlap with the approximate mode from within this subspace with eigenvalue $i\,e_0(L)$. The overlap approaches 1 for $\kappa \to 0^+$, and thus $\hat{l}_2$ stems from this subspace. Furthermore, it does not vanish for the whole parameter range, and as a consequence $\hat{l}_2$ is oddly transforming. These findings are independent of the system specifications. Note especially, that slowly increasing the interaction $U$ as $\kappa$ does not affect the general structure. Thus, we can treat the on-site interaction term in the same fashion as the dissipator by perturbation theory. The data has been generated with $J = 1$ and using exact diagonalization (ED).

proceed in the same way as the main theorem, as also depicted in Fig. S2. For this, notice that the interaction Hamiltonian also preserves the inversion symmetry. Thus, the main theorem stays valid.

Note that the arguments outlined above can be generalized to higher dimensions. For instance, in 2D, it can be shown that the Lindbladian again features an inversion symmetry of the two spatial coordinates. The main difference to the 1D case lies in the spectrum of the Hamiltonian, whose degeneracy strongly increases with the dimension. This makes the proof of the main theorem more involved and will be the subject of future studies. Nonetheless, exact diagonalization (ED) results for small-scale systems indicate that the symmetrically-localized (SL) state which we considered in the main text, converges to the Bose-Einstein condensate (BEC) exponentially faster than typical random states also in 2D.

## S2. UNITARY EQUIVALENCE BETWEEN LINDBLADIANS WITH DIFFERENT MOMENTA

In Section S1, we only considered Lindbladians with zero characteristic momentum $k_0 = 0$. Instead of solely generalizing the arguments given before to the arbitrary $k_0$ (which is possible), here we show that an even stronger connection exists between the different Lindbladians. This is done by introducing unitaries, transforming the different Lindbladians into each other. As a consequence, they share the same spectrum and their eigenmodes are connected.

Consider the unitary $\hat{U}_{k_0}$ acting on creation operators as

$$\hat{U}_{k_0}\hat{b}_j^\dagger \hat{U}_{k_0}^\dagger = \mathrm{e}^{\mathrm{i}k_0 j}\hat{b}_j^\dagger . \tag{S19}$$

This unitary has the physical interpretation of shifting the momentum by $k_0$. To identify the transformation behavior of the Lindbladian, we study the Hamiltonian and jump operators separately. The Hamiltonian transforms as

$$\hat{U}_{k_0}\hat{H}_{k=0}(J,U)\hat{U}_{k_0}^\dagger = \hat{H}_{k=k_0}(\sigma_{k_0}J,U) , \tag{S20}$$

and the jump operators obey

$$\hat{U}_{k_0}\hat{L}_j^{k=0}\hat{U}_{k_0}^\dagger = \hat{L}_j^{k=k_0} . \tag{S21}$$

Thus, the Lindbladians at different momenta are unitarily connected through the unitary $\hat{\mathcal{U}}_{k_0} = \hat{U}_{k_0} \otimes \hat{U}_{k_0}^*$, which is the vectorized version $\hat{U}_{k_0}$. As a consequence, the Lindbladian spectra are independent of the targeted momentum $k_0$. The eigenmodes are also related as

$$|r_j^{k=k_0}\rangle\!\rangle = \hat{\mathcal{U}}_{k_0}|r_j^{k=0}\rangle\!\rangle, \ \langle\!\langle l_j^{k=k_0}| = \langle\!\langle l_j^{k=0}|\hat{\mathcal{U}}_{k_0}^\dagger . \tag{S22}$$

The one-body density matrix $\boldsymbol{\gamma}_{ij} = \langle\hat{b}_j^\dagger\hat{b}_i\rangle$ is a valuable tool for quantitatively assessing the properties of the steady state. In the case of a finite-momentum BEC, it gives information about the condensate density and the momentum through its spectral decomposition. Due to the unitary relation between the right eigenmodes, $\boldsymbol{\gamma}$ is particularly simple. By inserting the unitary relation, using the cyclicity of the trace and the definition of $\hat{U}_{k_0}$, one finds

$$\boldsymbol{\gamma}_{lm}^{k_0} = \mathrm{Tr}\big(\hat{r}_1^{k_0}\hat{b}_m^\dagger\hat{b}_l\big) = e^{ik_0(m-l)}\mathrm{Tr}\big(\hat{r}_1^0\hat{b}_m^\dagger\hat{b}_l\big) . \tag{S23}$$

Fourier-transforming $\boldsymbol{\gamma}$ to momentum space gives

$$\boldsymbol{\gamma}_{k,k'}^{k_0} = \boldsymbol{\gamma}_{k+k_0,k'+k_0}^0 , \tag{S24}$$

which shows a unitary connection between $\boldsymbol{\gamma}^{k_0}$ and $\boldsymbol{\gamma}^0$. This relation is also consistent with the physical interpretation of the unitary transformation, shifting all momenta by $k_0$. Thus, the eigenvalues are the same, and the eigenmodes are connected by an index shift of $k_0$. Consequently, the condensate density only depends on wether $|k_0| < \pi/2$ or $|k_0| \geq \pi/2$.

Furthermore, the unitary affects the symmetry properties of $\hat{l}_2^{k_0}$. Luckily, they can be deduced easily from the inversion symmetry of the $k_0 = 0$ case by transforming with the unitary connection. This gives rise to a symmetry of the Hamiltonian, which depends on the targeted momentum $k_0$,

$$\hat{U}_{\text{inv}}^{k_0} = \hat{U}_{k_0} \hat{U}_{\text{inv}} \hat{U}_{k_0}^\dagger . \quad \text{(S25)}$$

Its action on creation operators is given by

$$\hat{U}_{\text{inv}}^{k_0} \hat{b}_j^\dagger \big(\hat{U}_{\text{inv}}^{k_0}\big)^\dagger = e^{ik_0(L+1)} e^{-2ik_0 j} \hat{b}_{L+1-j}^\dagger . \quad \text{(S26)}$$

The symmetric product states introduced before are again eigenstates of this symmetry and transform evenly as before. Also, $\hat{l}_2^{k_0}$ again transforms oddly, which implies that symmetric states will equilibrate exponentially faster than random states for arbitrary momenta $k_0$.

The Lindbladians for $|k_0| < \pi/2$ and $|k_0| \geq \pi/2$ are also connected unitarily; however, the hopping amplitude changes sign. To better understand this physically, we can introduce a further unitary to move the changed sign into the onsite interaction $U$. We will restrict our analysis to the case of $k_0 = \pi$ out of convenience, but the arguments can be readily generalized to other momenta. This time, it is beneficial to work directly on the vectorized Hilbert space. To avoid confusion, we will denote creation (annihilation) operators on the physical sublattice by $\hat{b}^\dagger$ ($\hat{b}$), and on the auxiliary sublattice by $\hat{a}^\dagger$ ($\hat{a}$). We define the unitary $\hat{S}$

$$\hat{S} \hat{a}_j \hat{S}^\dagger = \hat{b}_j , \quad \hat{S} \hat{b}_j \hat{S}^\dagger = \hat{a}_j . \quad \text{(S27)}$$

Denoting by $\hat{\mathcal{H}}_\pi(J, U)$ (we write the parameter dependence explicitly here, since it plays a major role) and $\hat{\mathcal{D}}_\pi$ the Hamiltonian and dissipative part of the Lindbladian $\hat{\mathcal{L}}_\pi$, respectively, we find the transformation behavior

$$\hat{S} \hat{\mathcal{H}}_\pi(J, U) \hat{S}^\dagger = \hat{\mathcal{H}}_\pi(-J, -U) , \quad \text{(S28)}$$

where we used the relation $\hat{H}_\pi^T(J, U) = \hat{H}_\pi(J, U)$. Notice that both $J$ and $U$ have changed their sign. Next, we use $\hat{L}_j^\pi = \big[L_j^\pi\big]^*$, where $*$ denotes a complex conjugation, to show

$$\hat{S} \hat{\mathcal{D}}_\pi \hat{S}^\dagger = \hat{\mathcal{D}}_\pi . \quad \text{(S29)}$$

This finally yields unitary equivalence between the Lindbladians

$$\hat{S} \big(\hat{\mathcal{H}}_\pi(J, U) + \hat{\mathcal{D}}_\pi\big) \hat{S}^\dagger = \big(\hat{\mathcal{H}}_\pi(-J, -U) + \hat{\mathcal{D}}_\pi\big) . \quad \text{(S30)}$$

Additionally, the pure product states $|\rho\rangle\rangle \sim \prod_j \big[\hat{a}_j^\dagger\big]^{N_j} \big[\hat{b}_j^\dagger\big]^{N_j} |\text{vac}\rangle\rangle$ are eigenstates of this unitary and therefore the convergence to the steady state is the same for both Lindbladians. If we now also use the unitary connection before, we find that

$$\hat{S}\hat{U}\big(\hat{\mathcal{H}}_0(J, U) + \hat{\mathcal{D}}_0\big)\hat{U}^\dagger \hat{S}^\dagger = \hat{\mathcal{H}}_\pi(J, -U) + \hat{\mathcal{D}}_\pi , \quad \text{(S31)}$$

and thus the Lindbladian at positive $U > 0$ and $|k_0| \geq \pi/2$ is unitarily connected to the ones with $U < 0$ and $|k_0| < \pi/2$. Moreover, $k_0 = \pi$ is especially interesting, since the Hamiltonian satisfies $\hat{H}_{k_0=0} = \hat{H}_{k_0=\pi}$ and only the jump operators are changed. Crucially, they are also real without phase modulations, and thus the experimental preparation of a BEC with momentum $k_0 = 0$ does not require any lattice shaking.

## S3. MEAN-FIELD THEORY AND PROPERTIES OF THE STEADY STATE

In contrast to adiabatic state preparation protocols, which directly prepare the ground state of some Hamiltonian without dissipative cooling, the dissipation strength $\kappa$ serves as an additional parameter controlling the preparation accuracy. In the following, we discuss the impact of $\kappa$ on the steady state analytically. Let us define $n = N/L$ and $n_0 = N_0/L$, where $N_0$ is the population of the zero-momentum mode, and we use the Fourier-transformed creation operators $\hat{b}_k^\dagger = 1/\sqrt{L} \sum_k e^{ikj} \hat{b}_j^\dagger$. To simplify the Lindbladian specified by Eqs. (S1) and (S11), we assume that $n - n_0/n = N - N_0/N \ll 1$. Then, we can make use of the Bogoliubov approximation $\hat{b}_0 = \sqrt{Ln_0} \approx \sqrt{Ln}$. Only keeping terms in the jump operators up to order $\sqrt{n}$, discarding boundary effects and observing that the summand with momentum $k = 0$ is zero yields $\hat{L}_k = 2\sqrt{n}(e^{ik} - 1)\hat{b}_k + \mathcal{O}(1)$. It is convenient to rotate the bosonic operators according to

$$\begin{pmatrix} \hat{c}_k \\ \hat{c}_{-k} \end{pmatrix} = \frac{1}{\sqrt{2}} \begin{pmatrix} 1 & 1 \\ -1 & 1 \end{pmatrix} \begin{pmatrix} \hat{b}_k \\ \hat{b}_{-k} \end{pmatrix} , \quad \text{(S32)}$$

to eliminate some couplings. Then, keeping only terms to order $n$ in the Hamiltonian, we find

$$\hat{H} = \sum_{k \neq 0} \left\{ (\epsilon_k + Un)\hat{c}_k^\dagger \hat{c}_k + \frac{Un}{2} \left( \big[\hat{c}_k\big]^2 + \big[\hat{c}_k^\dagger\big]^2 \right) \right\}, \quad \text{(S33)}$$

where we defined the non-interacting one-particle energies $\epsilon_k = 4J \sin^2 (k/2)$. The jump operators read

$$\hat{L}_k = \sqrt{\kappa_k} \hat{c}_k , \quad \kappa_k = 16n\kappa \sin^2 (k/2) . \quad \text{(S34)}$$

Accordingly, the master equation decouples and it can be solved for each $k$ separately [2]. The steady state is given by the mixed state

$$\hat{\rho}_{\text{ss}} = Z^{-1} \prod_{k \neq 0} e^{-\beta_k \hat{a}_k^\dagger \hat{a}_k} , \quad \text{(S35)}$$

with rotated bosonic operators $\hat{a}_k = \mathrm{e}^{-\mathrm{i}\phi_k}\cosh\theta_k\,\hat{c}_k + \mathrm{e}^{\mathrm{i}\phi_k}\sinh\theta_k\,\hat{c}_k^{\dagger}$. The parameters are given by

$$\cosh^2\left(2\theta_k\right) = \coth^2\left(\beta_k/2\right) = 1 + \frac{(Un)^2}{(1+a^2)E_k^2}\ , \quad \text{(S36)}$$

with the rescaled Bogoliubov energy $E_k = \sqrt{\epsilon_k^2 + 2Un\epsilon_k/(1+a^2)}$, where we defined the dimensionless constant $a = 2\kappa n/J$ and the phase reads

$$\cot(2\phi_k) = 2(\epsilon_k + Un)/\kappa_k\ . \quad \text{(S37)}$$

Note that the equation for the phase Eq. (S37) always has a solution, while Eq. (S36) has a solution $U > 0$, and care needs to be taken in case of $U < 0$, for which the constraint for existence of $\theta_k$ reads

$$\sin^2\left(k/2\right) > \frac{|U|Jn}{J^2 + (2n\kappa)^2}\ , \quad \forall\,k > 2\pi/L\ . \quad \text{(S38)}$$

This is fulfilled in particular in the two limits $\kappa \to \infty$ and $N \to \infty$ at constant $L$.

The steady-state Eq. (S35) is reminiscent of a thermal state. In the limit $(Un)^2/((1+a^2)E_k^2) \gg 0$, the expression simplifies to

$$\beta_k = \frac{E_k}{T_{\mathrm{eff}}}\ , \qquad T_{\mathrm{eff}} = \frac{UJn}{2\sqrt{J^2 + (4n\kappa)^2}}\ . \quad \text{(S39)}$$

Consequently, in this limit, the state is identical to the thermal state of an effective Bogoliubov Hamiltonian $\hat{H}_{\mathrm{eff}}$ at effective temperature $T_{\mathrm{eff}}$. Here, $\hat{H}_{\mathrm{eff}}$ is the Bose-Hubbard Hamiltonian Eq. (S1) with renormalized interaction strength $U_{\mathrm{eff}} = U/(1+a^2) < U$. This approximation works particularly well for long wavelengths $k \to 0$.

We are now equipped to study the behavior of the condensate depletion. In terms of the system parameters, it can be expressed as

$$\delta = \frac{1}{N}\sum_{k\neq0}\mathrm{Tr}\left(\hat{b}_k^{\dagger}\hat{b}_k\hat{\rho}_{\mathrm{ss}}\right) = \frac{1}{2N}\sum_k\frac{(Un)^2}{(1+a^2)E_k^2}\ . \quad \text{(S40)}$$

Crucially, it scales as

$$\delta = \mathcal{O}\left((U/\kappa)^2\,1/N\right)\ \text{ for }\ \kappa/J \gg \frac{L\sqrt{U}}{2\pi\sqrt{2nJ}}\ , \quad \text{(S41)}$$

which includes the two limits $N \to \infty$ and $\kappa \to \infty$. This explicitly shows that a strong dissipation counters interaction effects and can drastically increase the fidelity of the prepared BEC.

Lastly, we are interested in the behavior of the off-diagonal elements of the one-body density matrix $\gamma_{lm} = \langle\hat{b}_m^{\dagger}\hat{b}_l\rangle$ for the largest length scale $|l - m| = L$. Interestingly, this is directly connected to the depletion, and we have

$$\gamma_{lm} = n_0 + \frac{1}{L}\sum_{k\neq0}\frac{(Un)^2}{2(1+a^2)E_k^2}\mathrm{e}^{\mathrm{i}(l-m)k}\ . \quad \text{(S42)}$$
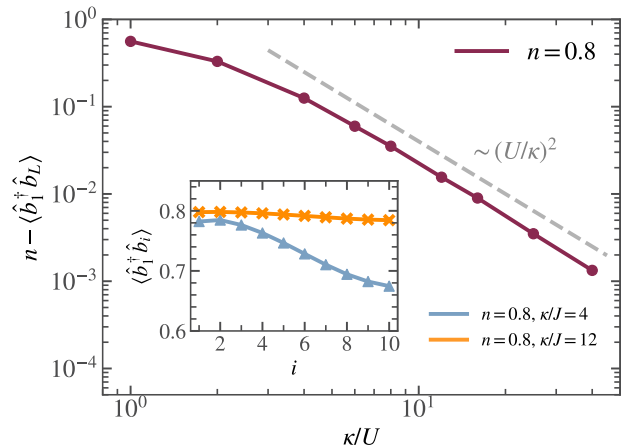


FIG. S3. Simulating the dissipative preparation of a BEC. We show the off-diagonal element $\gamma_{1L}$ of the one-body density matrix for several $\kappa/U$. We recover the scaling Eq. (S43), as predicted by Bogoliubov theory. This shows that the steady state features a lattice analogue of long-range order. Inset: Off-diagonal elements of the one-body density matrix for two different $\kappa/U$. All calculations were performed with the parameters $L = 10$, $N = 8$, $U = 1$ and $J = 1$, as well as $k_0 = 0$. The local dimension was set to $d = N + 1$.

Through a naive bound on the sum, we get

$$\gamma_{lm} > n(1 - 2\delta) = n - \mathcal{O}\left((U/\kappa)^2\right)\ . \quad \text{(S43)}$$

This can be understood as a long-range order in the limits $\kappa \to \infty$ or equivalently $N \to \infty$ at constant $L$. As we show in Fig. S3, this behavior is also found when simulating the dynamics with the full Lindbladian.

Notice, that all of this analysis carries over to the finite $k_0$-case, because of the unitary equivalences discussed in Section S2 and the validity of the approximation for general $U \neq 0$ (at least in the parameter regimes mentioned above).

## S4. NUMERICAL IMPLEMENTATION OF THE DISSIPATIVE DYNAMICS

Here, we provide the details of the numerical implementation of the dissipative time evolution considered in the main text. We employ the MPS representation [3] and vectorize the density matrices by doubling the system size, alternating physical and auxiliary sites, as shown schematically in Fig. S4. This arrangement of the sites avoids introducing long-range terms [4] in the MPO representation of the vectorized Lindbladian [5] (see Eq. (S10)). We compute the dissipative dynamics employing the time-dependent variational principle (TDVP) method for MPS [6, 7]. For highly-excited bosonic systems, characterized by large local physical dimension $d$, the most effective variant is the local subspace expansion time-dependent variational prin-
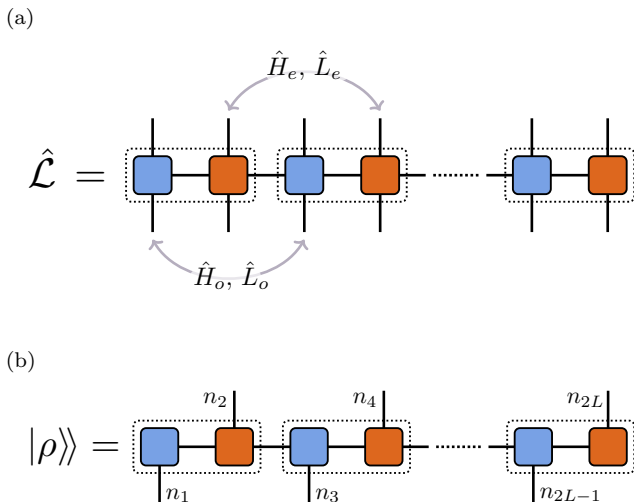
(a)



(b)

FIG. S4. The MPO representation of a vectorized Lindbladian (panel a) and of the MPS representation of a vectorized density matrix (panel b). Vectorization is carried out by purifying the system, i.e. adding an auxiliary site, marked in orange, for every physical site (colored blue). To ensure that the Lindbladian has only local terms, physical and auxiliary sites are alternated. Terms in Eq. (S10) that are on the left (right) of a tensor product act on odd (even) sites respectively and are indexed by o (e) accordingly. For the dissipative dynamics of a bosonic system that we consider here, the Hamiltonian and the jump operators feature next-nearest neighbor hopping.
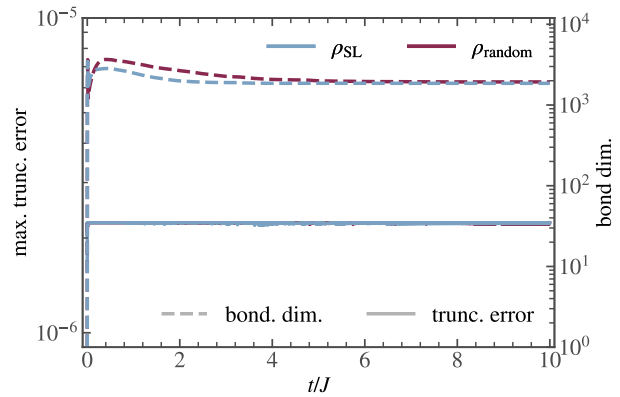


FIG. S5. Truncation error and right bond dimension for the Bose-Hubbard model with 10 sites and 10 particles, with $U/J = 0$ and $\kappa/J = 2$. For both initial states, there is a massive increase in bond dimension in the first time steps; later, it saturates at about 2000. To accurately capture the changes in the first steps, the time step was set to 0.0005, and after 20 steps it was increased to 0.005. The truncation error stays constant at about $2 \times 10^{-6}$.

ciple (LSE-TDVP) [8, 9]. This is based on single-site updates combined with a local subspace expansion [10], and is thus faster than the conventional two-site time-dependent variational principle (2TDVP) by a factor of $d$. We emphasize that care needs to be taken when using TDVP for Lindbladians, since they are non-Hermitian. In this context, two possible strategies are to either decompose the Lindbladian into a Hermitian and an anti-Hermitian part and to alternate real and imaginary Trotterized time steps or to perform a brute-force Taylor expansion of the exponentials of the local site tensors, as detailed in [11]. We followed the latter strategy.

To compute the dissipative dynamics efficiently, it is imperative to exploit the system's symmetries. First, note that the Lindbladian specified by the unitary part Eq. (S1) and the dissipative component Eq. (S11) conserve the total number of particles, and thus possess a corresponding global $U(1)$ symmetry. Moreover, since neither coherent nor dissipative hopping exchange particles between the physical and auxiliary sites (see panel a in Fig. S4), $\mathcal{L}$ possesses a second $U(1)$ symmetry associated with the particle conservation on the sublattices. This second symmetry only exists in the vectorized system and guarantees, that physical states are not connected to unphysical ones, which appear due to the enlargement of the Hilbert space. We exploit both the symmetries to obtain a block-decomposition of the Lindbladian. Furthermore, these symmetries ensure that at

most $N$ particles can sit on each site in the vectorized lattice (though $2N$ particles are on the lattice in total), allowing us to choose local dimension $d = N + 1$.

Due to the strong increase in bond dimension in the first few time steps, especially when starting from a pure product state, we initially use a small time step of $5 \times 10^{-4}$ and increase after 20 steps to either 0.01 or 0.005 (for some big calculations also 0.002), depending on system size. We track the norm of the time-evolved state, which needs to stay smaller than 1 to ensure a proper, physical evolution. We also track the maximal truncation error, which is defined as the maximal discarded weight [7] on a single site. In Fig. S5 we display the bond dimension (right axis) and the maximal truncation error (left axis) for one dissipative evolution considered in the main text. Notice that due to the symmetries discussed in Section S2, it is enough to perform calculations at zero characteristic momentum $k_0$. All calculations were performed using the SYTEN toolkit [12, 13].

Many studies of the Mpemba effect based on ED, employ the quantum relative entropy as a (pseudo) measure of distance from the steady state, whose exponential decay follows the exponent of the slowest-decaying mode [14, 15]. However, such a quantity is very difficult to compute in the MPS-vectorized framework. The only distance measure that is straightforward to compute in this picture is the $L_2$-norm

$$\|\hat{\rho}_1 - \hat{\rho}_2\|_2^2 = \text{Tr}\big((\hat{\rho}_1 - \hat{\rho}_2)^2\big) = \langle\!\langle\hat{\rho}_1 - \hat{\rho}_2|\hat{\rho}_1 - \hat{\rho}_2\rangle\!\rangle. \quad (S44)$$

This norm will show the exponential equilibration accurately. To see this, note that at a late time $t \gg 1/\text{Re}(\lambda_2)$, the time evolved state is accurately approximated by $\hat{\rho}(t) = \hat{\rho}_{ss} + a_2 e^{\lambda_2 t}\hat{r}_2 + \mathcal{O}\big(e^{t\,\text{Re}(\lambda_3)}\big)$. Thus, we imme-
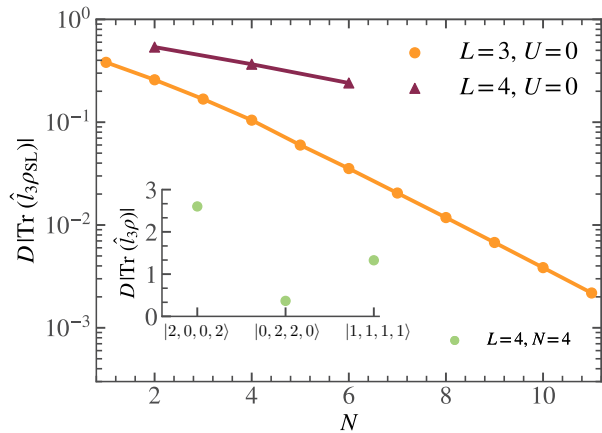
FIG. S6. Normalized overlap of the symmetrically-localized (SL) state with the second-slowest-decaying mode $\hat{l}_3$. The overlap vanishes exponentially with the number of bosons $N$, and thus, the convergence rate gets better upon increasing $N$. Inset: Overlap of the different symmetric states with $\hat{l}_3$ for the system specification $L = 4$, $N = 4$. The SL-state (i.e. $|0, 2, 2, 0\rangle$) has the smallest overlap with $\hat{l}_3$, making it the ideal initial state among all symmetric states. But also the constant density state $|1, 1, 1, 1\rangle$ has low overlap. For all calculations, we used the parameters $\kappa = J$ and $U = 0$ and ED to find the eigenmodes.

diately get that

$$\|\hat{\rho}(t) - \hat{\rho}_{ss}\|_2 = e^{t\,\mathrm{Re}(\lambda_2)}|a_2|\,\|\hat{r}_2^2\|_2 + \mathcal{O}\left(e^{t\,\mathrm{Re}(\lambda_3)}\right), \quad (S45)$$

which is exponential with rate $\mathrm{Re}(\lambda_2)$. For all our MPS-calculations, we obtain the steady state by a long-time evolution. Although this leads to an approximate steady state $\hat{\rho}_{ss} \approx \hat{\rho}(t_{max})$, we can track if it is sufficiently converged, by seeing if $\|\hat{\rho}(t) - \hat{\rho}_{ss}\|_2$ stays the same when considering $\hat{\rho}(t_{max})$ and $\hat{\rho}(t_{max} - \Delta t)$ as the steady state for a sufficiently big $\Delta t$. A similar analysis can be prformed by looking at the leading eigenvalue $N_0$ of the one-body density matrix $\gamma$ for $t_{max}$ and $t_{max} - \Delta t$.

The enforcing of normalization for density matrices presents another difficulty: In the vectorized picture, the normalization corresponds to

$$1 = \mathrm{Tr}(\hat{\rho}) = \langle\!\langle \hat{\mathbb{1}}|\hat{\rho}\rangle\!\rangle. \quad (S46)$$

Unfortunately, $|\mathbb{1}\rangle\!\rangle$ is a strongly entangled state and thus requires high bond dimensions. However, we can make use of the $U(1)$-symmetries and only calculate the state in one particular particle sector [7]. We define the operator

$$\hat{C}_{tot} = \sum_{j=1}^{L} \hat{b}_{2j}^\dagger \hat{b}_{2j+1}^\dagger. \quad (S47)$$

Then the vectorized identity in the N-particle sector is given by

$$|\mathbb{1}\rangle\!\rangle = \frac{1}{N!}\hat{C}_{tot}^N |\mathrm{vac}\rangle. \quad (S48)$$

This relation is easily proven using the multinomial theorem.

Finally, we focus on the equilibration behaviour of different symmetric initial states. As discussed in Section S1, we identified a class of exponentially faster-equilibrating states, namely those that are invariant under reflections about the center of the lattice. We are mainly interested in those, which are also pure-product states, as they are especially useful in experimental realizations. Among these states, the fastest-equilibrating one is the symmetric state that has the lowest overlap with the second-slowest decaying mode $\hat{l}_3$. To be able to compare different system specifications with each other quantitatively, we need to normalize $\hat{l}_3$, such that the sum over absolute values of the diagonal elements is equal to one. Then, we multiply with the Hilbert space dimension $D$ to get a comparable quantity that fulfills

$$D\left|\mathrm{Tr}(\hat{l}_3\hat{\rho}_{random})\right| = 1, \quad (S49)$$

when averaging over many $\hat{\rho}_{random}$. In Fig. S6, using ED we show that the overlap of the SL state (having all bosons located on the central sites) with $\hat{l}_3$ decays exponentially with $N$. This helps explaining why in Fig. 3b in the main text the speedups remain approximately constant upon increasing the system size, despite the fact that the Lindbladian spectrum becomes denser. Moreover, the inset indicates that the SL state has the smallest overlap with $\hat{l}_3$ among all symmetric states.

[S1] Gabriel T. Landi, Dario Poletti, and Gernot Schaller, "Nonequilibrium boundary-driven quantum systems: Models, methods, and properties," Rev. Mod. Phys. **94**, 045006 (2022).

[S2] S Diehl, A Micheli, A Kantian, B Kraus, H P Büchler, and P Zoller, "Quantum states and phases in driven open quantum systems with cold atoms," Nature Physics **4**, 878–883 (2008).

[S3] U. Schollwöck, "The density-matrix renormalization

group in the age of matrix product states," Ann. Phys. **326**, 96 (2011).

[S4] Heitor P. Casagrande, Dario Poletti, and Gabriel T. Landi, "Analysis of a density matrix renormalization group approach for transport in open quantum systems," Computer Physics Communications **267**, 108060 (2021).

[S5] Stefan Wolff, Ameneh Sheikhan, and Corinna Kollath, "Numerical evaluation of two-time correlation functions

in open quantum systems with matrix product state methods: a comparison," SciPost Phys. Core **3**, 010 (2020).

[S6] Jutho Haegeman, J. Ignacio Cirac, Tobias J. Osborne, Iztok Pižorn, Henri Verschelde, and Frank Verstraete, "Time-dependent variational principle for quantum lattices," Phys. Rev. Lett. **107**, 070601 (2011).

[S7] Sebastian Paeckel, Thomas Köhler, Andreas Swoboda, Salvatore R. Manmana, Ulrich Schollwöck, and Claudius Hubig, "Time-evolution methods for matrix-product states," Ann. Phys. **411**, 167998 (2019).

[S8] M. Yang and S. R. White, "Time-dependent variational principle with ancillary Krylov subspace," Phys. Rev. B **102** (2020).

[S9] Martin Grundner, Tizian Blatz, John Sous, Ulrich Schollwöck, and Sebastian Paeckel, (2023), arXiv:2308.13427 [cond-mat.supr-con].

[S10] C. Hubig, I. P. McCulloch, U. Schollwöck, and F. A. Wolf, "Strictly single-site dmrg algorithm with subspace expansion," Phys. Rev. B **91**, 155115 (2015).

[S11] Mattia Moroder, "Simulating quantum dissipative and vibrational environments," (2024).

[S12] Claudius Hubig, Felix Lachenmaier, Nils-Oliver Linden, Teresa Reinhard, Leo Stenzel, Andreas Swoboda, Martin Grundner, and Sam Mardazad, "The SyTen toolkit," .

[S13] Claudius Hubig, *Symmetry-Protected Tensor Networks*, Ph.D. thesis, LMU München (2017).

[S14] Mattia Moroder, Oisín Culhane, Krissia Zawadzki, and John Goold, "Thermodynamics of the quantum mpemba effect," Phys. Rev. Lett. **133**, 140404 (2024).

[S15] Juliane Graf, Janine Splettstoesser, and Juliette Monsel, "Role of electron-electron interaction in the mpemba effect in quantum dots," (2025), arXiv:2412.18456 [cond-mat.mes-hall].